Inorganic Chemistry

Article

pubs.acs.org/IC

α-Substituted Bis(octabutoxyphthalocyaninato)Terbium(III) Double-Decker Complexes: Preparation and Study of Protonation by NMR and DFT

Marko Damjanović,[†] Yusuke Horie,[‡] Takaumi Morita,[‡] Yoji Horii,[‡] Keiichi Katoh,*[,‡,§] Masahiro Yamashita,*[,‡,§] and Markus Enders*[,†]

[†]Institute of Inorganic Chemistry, University of Heidelberg, Im Neuenheimer Feld 270, D-69120 Heidelberg, Germany

[‡]Department of Chemistry, Graduate School of Science, Tohoku University, 6-3, Aramaki-Aza-Aoba, Aoba-ku, Sendai, Miyagi 980-8578, Japan

[§]CREST, JST, 4-1-8, Honcho, Kawaguchi, Saitama 332-0012, Japan

Supporting Information

ABSTRACT: Synthesis of the anionic, α-substituted, bis(phthalocyaninato)Tb^{III} complex [Tb(α-obPc)$_2$]$^-$ ([**1**]$^-$) (obPc = α-octabutoxyphthalocyaninato) leads to the isolation of its protonated form [**1**H]^0. This complex was characterized by X-ray diffraction (XRD), mass spectroscopy (MS), infrared (IR) and ultraviolet−visible−near-infrared (UV−vis-NIR) spectroscopy. Crystal structure analysis did not allow localization of the additional proton, which is probably attached to the *meso*-N atom or isoindole-N atom of the phthalocyaninato ligand. [**1**H]^0 can easily be deprotonated or protonated, giving the corresponding anionic and cationic complexes. The three compounds [**1**H]^0, [**1**]$^-$, and [**1**HH]$^+$ were studied by a combination of paramagnetic NMR experiments (^{1}H, ^{13}C, variable-temperature measurements, two-dimensional nuclear magnetic resonance and DFT calculations (done on Y^{III} analogues with octamethoxyphthalocyaninato ligands), for the purpose of elucidating the positions of the acidic protons and for understanding the structural changes of the coordination environment of the Tb ion induced by protonation.

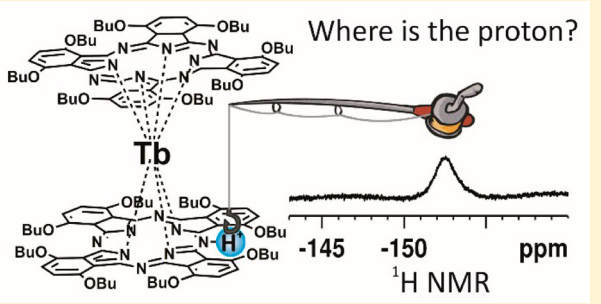

1. INTRODUCTION

The discovery of single-molecule magnets (SMMs) in 1993[1] made a significant impact on the course of materials science. SMMs possess a magnetic bistability on the molecular level and quantum effects that cannot be seen in classical bulk magnets. Today, great efforts are made toward pushing the frontiers of SMMs, through the design of complexes with increased blocking temperatures and suppressed magnetic relaxation processes.[2] SMMs attract great attention, because of their potential application for ultrahigh density molecular memories and for quantum bits (qubits). In particular, the unsubstituted Tb^{III}−phthalocyaninato double-decker complex TbPc$_2$ shows unparalleled SMM properties.[3] Because of its large activation energy for spin reversal (ca. 400 cm^{-1}) and high chemical stability, TbPc$_2$ has been used for research in spintronic devices.[4] It is well-known that TbPc$_2$ analogues also show good SMM properties. Ogawa and co-workers reported the SMM properties of Tb^{III}−tetraphenylporphyrinato (TPP) double-decker complexes Tb(TPP)$_2$ and TbH(TPP)$_2$, which are the analogues of TbPc$_2$.[5] With the help of single-crystal X-ray analysis of TbH(TPP)$_2$, the position of protons connected to the pyrrole ring was determined for the first time, and the distorted square antiprismatic (SAP) coordination mode around Tb^{III} in TbH(TPP)$_2$ was shown as well. Because of the distortion and low symmetry in TbH(TPP)$_2$, this complex did not show SMM properties. In contrast, the deprotonated complex showed SMM properties, because of the highly symmetric SAP coordination. Thus, these complexes achieve a proton-induced switching of SMM properties by a reversible protonation−deprotonation. In the case of the protonated Tb^{III}−phthalocyaninato−porphyrinato heteroleptic double-decker complex Tb(TPP)(HPc), an acidic proton is located on the *meso*-N atom of the phthalocyanine ligand.[6] Since the acidic proton did not disturb the SAP coordination geometry around Tb^{III} ions, Tb(TPP)(HPc) keeps its SMM properties. Although the positions of the protons of TbH(TPP)$_2$ and Tb(TPP)(HPc) were determined by single-crystal X-ray structural analysis, it is still difficult to determine the position of the acidic proton directly, because of its low electron density. On the other hand, ^{1}H NMR measurements are highly sensitive and can directly reveal the position of the proton via analysis of its paramagnetic NMR shift, as will be shown in this work.

Received: October 16, 2015
Published: December 9, 2015

DOI: 10.1021/acs.inorgchem.5b02391
Inorg. Chem. 2015, 54, 11986−11992

Recently, our research group has reported the nuclear magnetic resonance (NMR) analysis of lanthanide SMMs.[7] Aided with various NMR experiments full assignments of the ^{1}H and ^{13}C resonances in Tb^{III}–β-butoxy substituted phthalocyaninato triple-decker complex $Tb_2(\beta\text{-obPc})_3$ and solution structure analysis has been achieved. In addition, redox series of double-decker complexes $[Tb(\beta\text{-obPc})_2]^{-/0/+}$ were investigated by ^{1}H and ^{13}C NMR measurements. A combination of NMR measurements and density functional theory (DFT) calculations enabled us not only to separate hyperfine shift contributions but also to determine the interligand distances in the $[Tb(\beta\text{-obPc})_2]^{+}$ complex, for which no crystal structure is available. In addition, the analysis showed that the π-radical and the unpaired f-electrons at Tb^{III} in the neutral $[Tb(\beta\text{-obPc})_2]^{0}$ complex are ferromagnetically coupled at room temperature.

On the basis of our previous research, here we report the synthesis, characterization, and a combined NMR- and DFT-based analysis of the new double-decker complex $[\mathbf{1}H]^{0}$ (Figure 1) and its deprotonated and protonated forms, respectively.

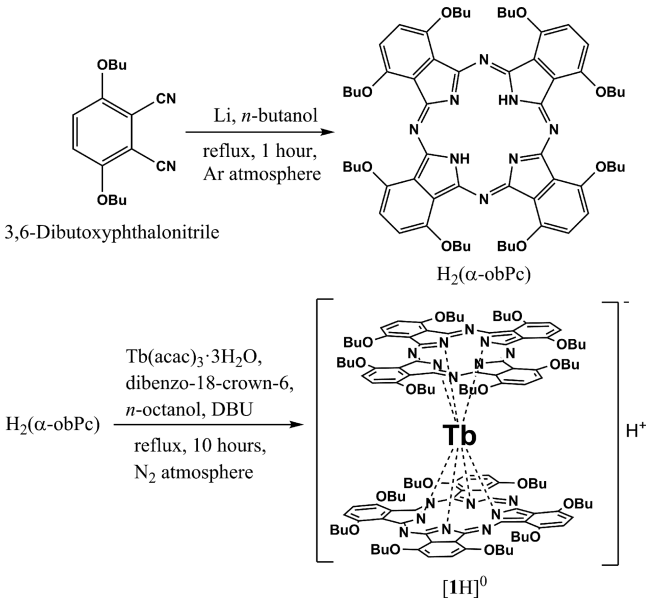

Figure 1. Schematic representation of the synthesis of $H_2(\alpha\text{-obPc})$ and of $[\mathbf{1}H]^{0}$ ($[Tb(\alpha\text{-obPc})_2H]^{0}$, where α-obPc is the dianion of 1,4,8,11,15,18,22,25-octa(*n*-butoxy)phthalocyaninato). The position of the acidic proton could not be determined from crystal structure data.

In 2010, Jiang and co-workers reported the synthesis and structural determination of $[M(\alpha\text{-obPcH})(\alpha\text{-obPc})]^{0}$ (M = Eu^{III} or Y^{III}) and deprotonated $[M(\alpha\text{-obPc})_2]^{-}$ complexes.[8] Single-crystal XRD measurements of $[Eu(\alpha\text{-obPcH})(\alpha\text{-obPc})]^{0}$ could not elucidate the position of the acidic proton.

In this article, we chose Tb^{III} ions as a metal center of the double-decker assembly to determine the position of acidic proton for the following reasons: (1) toward the improved understanding of the factors that lead to emergence of SMM properties, (2) Tb^{III}–phthalocyaninato complexes have strong uniaxial magnetic anisotropies, which makes NMR analysis easier. Paramagnetic shifts in ^{1}H NMR of lanthanoid systems are dominated by the pseudo-contact shift (PCS), which is quite sensitive to the atomic coordinates. Therefore, the position of acidic protons can be determined by analysis of paramagnetic NMR shifts. In addition to these experiments, we report the synthesis and NMR analysis of $[Tb(\alpha\text{-obPcH})_2]^{+}$ ($[\mathbf{1}HH]^{+}$), which is the first example of a doubly protonated double-decker structure.

2. EXPERIMENTAL DETAILS

2.1. General Information. The required reagents and solvents were used as provided by the supplier, without further purification. 1,8-Diazabicyclo[5.4.0]-undec-7-ene (DBU), 1-butanol, and 1-octanol were purchased from Wako Chemicals. Metal lithium wire (3 mm in diameter) and dibenzo-18-crown-6 were purchased from Sigma–Aldrich. Tb^{III} acetylacetonate trihydrate $Tb(acac)_3{\cdot}3H_2O$ was purchased from Strem Chemicals. The solvents used for column chromatography were special grade from Wako Chemicals. 3,6-Dibutoxyphthalonitrile was synthesized according to a reported method.[9]

2.2. Synthesis of $[Tb(\alpha\text{-obPc})_2H]^{0}$ ($[\mathbf{1}H]^{0}$). The complex was prepared by modifying a reported procedure for isostructural Eu^{III} and Y^{III} complexes.[8] $H_2(\alpha\text{-obPc})$ was prepared according to a previously reported procedure (see the Supporting Information).[9] Figure 1 shows the synthesis of the $H_2(\alpha\text{-obPc})$ ligand and, subsequently, the synthesis of $[\mathbf{1}H]^{0}$. $H_2(\alpha\text{-obPc})$ (171 mg, 0.156 mmol), $Tb(acac)_3{\cdot}3H_2O$ (36 mg, 0.0727 mmol), dibenzo-18-crown-6 (29 mg, 0.0804 mmol) and DBU (3 mL) were refluxed for 10 h in *n*-octanol (16 mL) under N_2 atmosphere. The mixture was evaporated under reduced pressure. The residue was chromatographed on a neutral alumina column (Al_2O_3, Merck) with $CHCl_3$ as an eluent. A deep green fraction was collected. After the solvent was evaporated, column chromatography was repeated over BioBeads S-X1 with tetrahydrofuran (THF) for further purification. Recrystallizing from toluene/MeOH gave a dark green powder (49 mg, 28.8%). ESI-MS: m/z 2338.15 (100%) $[M]^{+}$ ($\equiv [\mathbf{1}H]^{+}$) (see Figure S1 in the Supporting Information). Elemental analysis for $C_{128}H_{161}N_{16}O_{16}Tb$ (%): Calcd.: C 65.73, H 6.93, N 9.58. Found: C 65.85, H 6.95, N 9.54.

2.3. Characterization of $[\mathbf{1}H]^{0}$. Before NMR measurements were conducted, $[\mathbf{1}H]^{0}$ was characterized by elemental analysis, electron spin ionization-mass spectroscopy (ESI-MS), ultraviolet–visible–near-infrared (UV-vis-NIR) spectroscopy, infrared (IR) analysis, and X-ray structural analysis. The molecular structure and the recorded spectra are shown in the Supporting Information (Figures S1–S4, and Table S1). Elemental analysis and MS measurements were performed at the Research and Analytical Centre for Giant Molecules, Tohoku University. UV-vis-NIR spectra were corrected on a Shimadzu Model UV-3100PC system, by using CH_2Cl_2 as a solvent. IR spectroscopy was performed on attenuated total reflection (ATR) method on Jasco FT/IR-4200. Single crystals suitable for SXRD measurements were made by slow diffusion of a $CHCl_3$ solution of the complex into toluene. The XRD data for $[\mathbf{1}H]^{0}$ were collected at 90 K on a Bruker APEX-II CCD diffractometer with graphite monochromated Mo Kα radiation (λ = 0.7107 Å). The crystal was mounted on the Micromount with Paratone-N. The initial structure of $[\mathbf{1}H]^{0}$ was solved by Intrinsic Phasing (Bruker APEX-II). Refinement by a full-matrix least-squares method on F^2 by using SHELX-97[10] was performed. All non-hydrogen atoms were refined anisotropically using a least-squares method, and hydrogen atoms were fixed at calculated position.

2.4. NMR Measurements. NMR spectra were recorded at a field strengths of 7.9 T (400 MHz) with a Bruker Avance II instrument equipped with a BBFO probe and at a field strength of 14.09 T (600 MHz) with a Bruker Avance III instrument equipped with a QNP Cryoprobe (inner coil tuned to ^{13}C, cold preamplifier). Prior to variable-temperature measurements, temperature calibration was done by using the temperature dependence of the residual nondeuterated methanol signal in deuterated methanol.[11] Solvent resonances were taken as references for all ^{1}H and ^{13}C NMR spectra.[12] Deuterated solvents (CD_2Cl_2 and toluene-d_8, Sigma–Aldrich) were dried with conventional methods (over CaH_2) and degassed before use with the freeze–pump–thaw technique. DBU and glacial acetic acid were used as provided by the supplier (Sigma–Aldrich). The sample with the anionic complex $[\mathbf{1}]^{-}$ (D_{4d} point group) was prepared by adding

DOI: 10.1021/acs.inorgchem.5b02391
Inorg. Chem. 2015, 54, 11986–11992

excess DBU to a toluene-d_8 solution of $[\mathbf{1}H]^0$. The sample with the doubly protonated complex, $[\mathbf{1}HH]^+$, was prepared by adding an excess of glacial acetic acid to a toluene-d_8 solution of $[\mathbf{1}H]^0$. All samples for NMR measurements were prepared and stored in an inert gas atmosphere, in NMR tubes with Teflon plugs (J. Young valves).

2.5. DFT Calculations. For the purpose of using computational resources reasonably, the density functional theory (DFT) calculations were performed with Y^{III} complexes, rather than with Tb^{III} complexes. This was done since it is known that the ionic radii of Y^{III} and Tb^{III} are almost equivalent (115.9 pm for Y^{III} vs 116.7 pm for Tb^{III}, for 8-coordinated complexes).[13] Furthermore, in the DFT calculations, butoxy substituents on the α-positions of the phthalocyaninato ligands were replaced with methoxy substituents (abbreviated as omPc, thus reducing the total number of atoms in each structure by a factor of ~1.9). DFT calculations were performed with the program Gaussian 09 (revision D.01).[14] Geometry optimizations were done with the restricted B3LYP functional.[15] The def2svp[16] basis set was used for all light atoms and Stuttgart ECP was used for Y^{III}.[17] In all geometry calculations, the dispersion interaction was included (Grimme DFT-D3 with Becke-Johnson damping).[18] The "superfine" integration grid was used throughout, and the quadratically convergent self-consistent field (SCF) procedure was utilized when convergence could not be achieved by the first-order SCF methodology.[19] Tight criteria were used for optimization. No symmetry restrictions were imposed during the optimization procedure. For all structures, stationary points on the potential energy surface were characterized as minima by the absence of imaginary frequencies. The validity of this geometry optimization strategy for phthalocyaninato double-decker complexes was previously shown by Kitagawa et al.[20] and in our recent NMR study of β-substituted octabutoxyphthalocyaninato Tb^{III} and Dy^{III} double-decker complexes.[7b] Single-point calculations of the optimized geometries were done using the restricted B3LYP functional and using the def2tzvp[16] basis set on all atoms. The "superfine" integration grid was used, along with the "scf = xqc" procedure. The *xyz* coordinates of the optimized structures, the energies from single-point calculations and the interligand distances of the various optimized structures (defined as the separation of the centroids of the two N_4 basal planes of the square antiprism) are provided in the Supporting Information.

3. RESULTS AND DISCUSSION

3.1. Characterization of $[1H]^0$. In the IR spectrum (Figure S2 in the Supporting Information), a weak peak at 3246 cm^{-1} is observed for $[\mathbf{1}H]^0$, which originates from the acidic proton, which is connected to a nitrogen atom. The lack of a broad peak at ~1500 nm in the UV-vis-NIR spectrum of $[\mathbf{1}H]^0$ (see Figure S3 in the Supporting Information) proves that no π-radical is present. The crystal structure of $[\mathbf{1}H]^0$ is given in Figure S4 in the Supporting Information (Cambridge Crystallographic Data Centre (CCDC) No. 1438573). This complex crystallizes in the monoclinic $P2_1/c$ group, with no solvent molecules incorporated in the structure. Despite considerable effort, the position of the acidic proton in the crystal structure could not be found. Skeletal π-structures of the α-obPc ligands are strongly distorted due to the steric hindrance induced via the *n*-butoxy chains in α-positions. The stacking angle between the phthalocyaninato ligands within a single molecule is 43.9°, corresponding to a staggered conformation. The Tb^{III} ion is located almost in the middle between the two ligands. As will be shown in the following sections, the nonprotonated α-obPc ligand is closer to the metal center than the α-obPcH one. The intermolecular $\pi-\pi$ interactions lead to a slipped column structure along the *c*-axis.

3.2. Analysis of NMR Data. A detailed introduction about the NMR analysis of Tb^{III}–phthalocyaninato complexes, and generally about NMR of paramagnetic complexes, has been given in our previous work,[7] in well-known works of Bertini et al.[21] and La Mar et al.,[22] and elsewhere.[23] Recently, a complete *ab initio* theory for paramagnetic NMR shifts that goes far beyond the simple eqs 1–4 has been developed.[23d–f] The dominant contribution to the hyperfine shift of ^1H nuclei in the complexes studied in this work is the pseudo-contact term (δ_{PC}), which can be described by a simple point-dipole based eq 1 for general cases and eq 2 for axially symmetric complexes:

$$\delta_{PC} = \frac{1}{12\pi}[\chi_a G + \chi_{rh} H] \quad (1)$$

$$\delta_{PC} = \frac{\chi_a G}{12\pi} \quad (2)$$

where χ_a and χ_{rh} are the axial and rhombic components of the magnetic susceptibility anisotropy tensor, respectively, and G and H are geometric factors expressed by the following relationships (eqs 3 and 4):

$$G = \frac{3\cos^2\theta - 1}{r^3} \quad (3)$$

$$H = \frac{3}{2}\left(\frac{\sin^2\theta\cos 2\Omega}{r^3}\right) \quad (4)$$

where r is the length of the vector connecting the Tb^{III} ion and the NMR nucleus, θ the angle between the corresponding r vector and the magnetic susceptibility main axis, and Ω the angle that the r vector makes in the plane perpendicular to the magnetic susceptibility axis. For complexes studied in this work, the rhombic component of the χ tensor is neglected because of the axial symmetry of the first coordination sphere of the metal, which leads to a simplified analysis.

The ^1H NMR spectrum of $[\mathbf{1}H]^0$ (Figure 2) is quite complicated, since protonation alleviates the D_{4d} symmetry of the anionic double-decker complex. The intense eight signals due to chemically inequivalent methyl groups can clearly be identified in the region from −5 ppm to −17 ppm. The diastereotopic $CH_2\alpha$, $CH_2\beta$, and $CH_2\gamma$ groups, along with eight CH_{ar} groups, give a total of 56 signals, some of which overlap

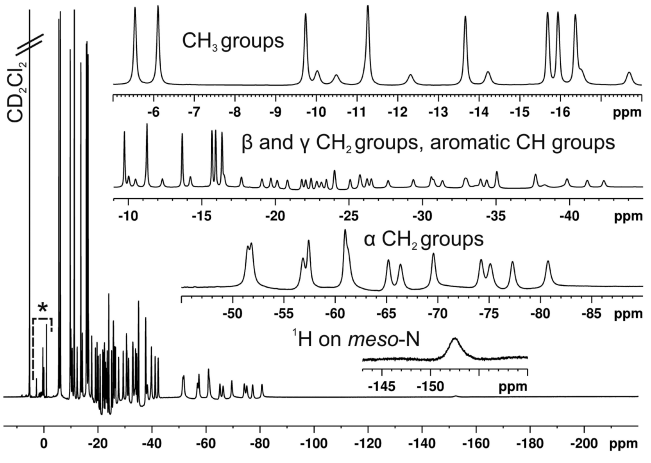

Figure 2. ^1H NMR spectrum of $[\mathbf{1}H]^0$ (295.0 K, CD_2Cl_2, 14.09 T). Upper inset: expanded region with signals of 8 methyl groups. Upper middle inset: expanded region with signals of diastereotopic $CH_2\beta$ and $CH_2\gamma$ groups. Lower middle inset: expanded region with signals of diastereotopic $CH_2\alpha$ groups. Lower inset: expanded region with the proton on the *meso*-N atom. Features marked by an asterisk (*) represent impurities.

DOI: 10.1021/acs.inorgchem.5b02391
Inorg. Chem. 2015, 54, 11986–11992

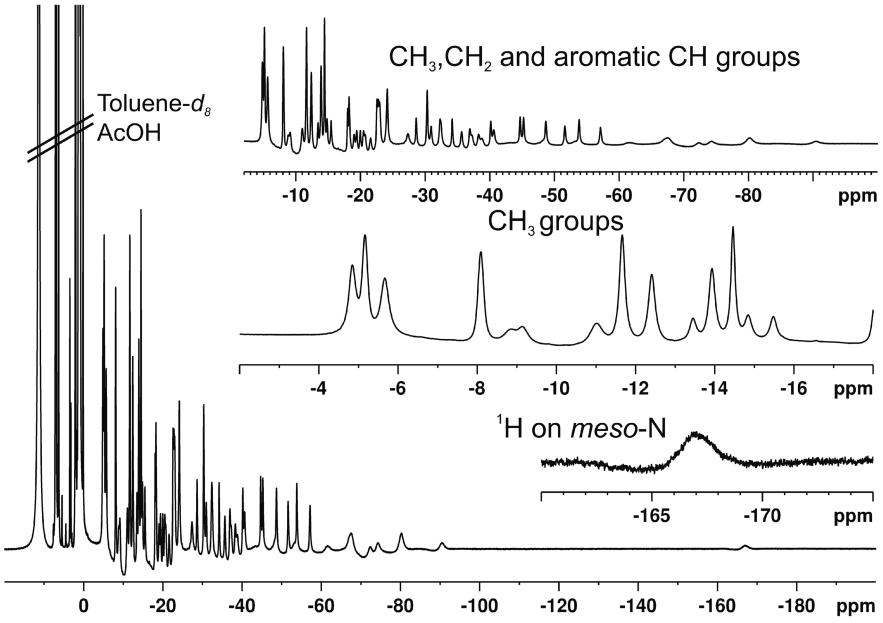

Figure 3. ^{1}H NMR spectrum of $[\mathbf{1}HH]^+[CH_3COO]^-$ by protonation of $[\mathbf{1}H]^0$ (295.0 K, toluene-d_8, 14.09 T). Upper inset: expanded region from −2 ppm to −100 ppm. Middle inset: expanded region with eight methyl group signals. Lower inset: expanded region from −160 ppm to −175 ppm.

but can be distinguished at elevated temperatures (see the Supporting Information). The most shifted signal in Figure 2, at −152.50 ppm, belongs to the acidic proton on the phthalocyaninato ligand. The sign and the magnitude of the hyperfine shift of the signal confirm that this proton is located on the *meso*-N. This is verified by DFT calculations, as will be shown in the next section. If the proton were located on an isoindole-N, due to the nature of eq 2, it would experience a very large and positive δ_{PC}. Namely, with the use of eq 2, it can easily be shown that a protonation on the *meso*-N atom would result in a δ_{PC} value of approximately −161.5 ppm, whereas an acidic proton on the isoindole-N atom would experience a δ_{PC} value of +2073.3 ppm (see the Supporting Information). No ^{1}H signal was observed in the chemical shift region at approximately +2000 ppm. The χ_a value of the studied $[\mathbf{1}H]^0$ complex was estimated to be 9.50×10^{-30} m^3 (see the Supporting Information), which is close to the value determined for the previously studied $[Tb(\beta\text{-obPc})_2]^-$ complex.[7b] An EXSY measurement of the less-crowded region of the spectrum, containing signals of the $CH_2\alpha$ groups, shows that at 380.0 K (in toluene-d_8), the $CH_2\alpha$ protons within the α-obPc ligand are exchanging with each other, which indicates ligand rotation. Studies of the dynamics in lanthanide complexes bearing porphyrinato ligands revealed that the ligand rotation barriers can be large (e.g., $Ce(MOTP)_2$, where MOTP is a porphyrinato-based ligand, $\Delta G^{\ddagger} = 101 \pm 0.4$ kJ mol^{-1} at 50 °C)[24] and inversely proportional to the interplanar spacing between porphyrinato ligands.[25] Hence, we expect that the rotation barrier in Tb^{III}−phthalocyaninato complexes is also high. Because of the low symmetry of $[\mathbf{1}H]^0$ and to the small differences in δ_{PC} of the resonances of the α-obPcH and α-obPc ligands, it is not possible to quantify the changes in ligand−metal distances that are induced by a protonation. However, as will be shown, DFT provides valuable insights into the structure of the title complex. Upon deprotonation with an excess of DBU (1,8-Diazabicyclo[5.4.0]undec-7-ene), $[\mathbf{1}]^-$ [H-DBU]$^+$ is obtained, which has simple ^{1}H and ^{13}C NMR spectra, because of the D_{4d} point group (see Figure S15 in the Supporting Information). The deprotonation is shown to be reversible via the addition of acetic acid. A second protonation with glacial acetic acid is possible, thereby inducing a color change of the complex from green to red. The ^{1}H NMR spectrum of the doubly protonated, now cationic complex, is shown in Figure 3.

The second protonation could also be observed in CD_2Cl_2, but it was not complete, even with a considerably excessive amount of acid. However, a complete double protonation is possible in toluene. As can be seen in Figure 3, a second protonation does not lead to an increase in the symmetry of the complex. The most negatively shifted signal corresponds to two acidic protons on *meso*-N atoms, and these ^{1}H resonances experience a larger δ_{PC} than the proton on the *meso*-N atom in $[\mathbf{1}H]^0$ (Figure 2). Unlike for $[\mathbf{1}]^-[H\text{-DBU}]^+$, the doubly protonated complex undergoes a dynamic process at higher temperatures (see the Supporting Information). This can be due to either a fast proton exchange process, or it could be due to a decreased ligand rotation barrier caused by the structural change induced by protonations. The distinction between these two dynamic processes cannot be made based solely on NMR data. However, a more-detailed understanding of the structure and molecular dynamics of the doubly protonated species is achieved with the help of DFT calculations, as will be shown in the next section.

3.3. Analysis of DFT Calculations. *3.3.1. Proton Position.* As the single-point calculations of the optimized geometries indicate, it is more favorable for the proton in $[Y(\alpha\text{-omPcH})(\alpha\text{-omPc})]$ to be located on the *meso*-N, rather than on the isoindole-N, by ca. 57 kJ/mol. This theoretical outcome is in agreement with the NMR data, which show that the *meso*-N atom is protonated in $[\mathbf{1}H]^0$. Our findings are in agreement with the recent study of a mixed Tb^{III}−(phthalocyaninato)(porphyrinato) double-decker complex, conducted by Tanaka et al.[6] The DFT structures were also used to determine structural parameters that are used in pseudo-contact shift (eq 2). The magnetic properties relevant for NMR spectroscopy, such as electronic *g*-factors, can be obtained from relativistic

DOI: 10.1021/acs.inorgchem.5b02391
Inorg. Chem. 2015, 54, 11986−11992

DFT calculations.[26] However, the existing methods are unlikely to be suitable for open-shell *f*-elements. An alternative to the experimental determination of the susceptibility anisotropy are the newly developed *ab initio* multireference wavefunction methods.[23e,f] The DFT calculations of the four possible permutations of proton positions on the *meso*-N atoms in the doubly protonated complex show that it is unlikely that the same α-obPc ligand gets protonated twice, and that the two protons are likely to be on *meso*-N atoms on different α-obPc ligands. This is shown in Figure 4, which depicts schematic representations of the four permutations.

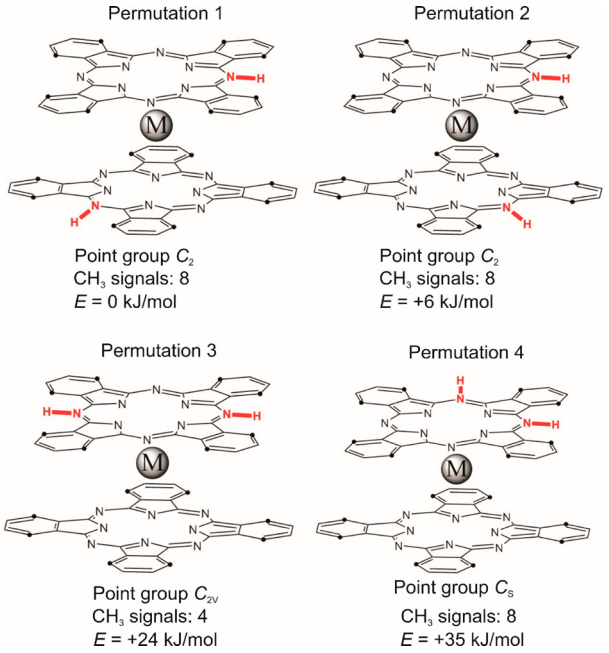

Figure 4. Schematic representation of four permutations that describe the position of the second proton in the cationic complex. For clarity reasons, the *ortho*-butoxy chains are represented by black dots. The point groups and number of expected signals for the methyl groups of the butoxy chains are given in the figure, as well as the relative energies, as obtained from single-point DFT calculations.

The $[Y(\alpha\text{-omPcH})_2]^+$ structure with the two protons being as far apart as possible (permutation 1) has the lowest energy. The $[Y(\alpha\text{-omPcH})_2]^+$ structure in which the two protons are located on nearby *meso*-N atoms is ~6 kJ/mol higher in energy (permutation 2). The $[Y(\alpha\text{-omPcH}_2)(\alpha\text{-omPc})]^+$ structures, in which the protons are located on opposite (permutation 3) or neighboring (permutation 4) *meso*-N atoms within the same ligand are ca. 24 kJ/mol and ca. 35 kJ/mol higher in energy than the structure with permutation 1, respectively. This theoretical outcome is in agreement with the experimental results obtained by NMR. Namely, a second protonation of the opposite *meso*-N position in the same α-obPc ligand (permutation 3, C_{2v} point group) would lead to an increased symmetry, which would result in a decrease in the total number of observed signals by NMR. The existence of the permutation 4 structure is unlikely, because of its very high energy cost. In $[\mathbf{1}H]^0$, the eight methyl group signals are due to four chemically inequivalent groups from each of the two ligands (C_s point group). On the other hand, in the C_2 symmetric permutations of $[\mathbf{1}HH]^+$, the eight methyl group signals stem from the eight chemically inequivalent methyl groups within a single α-obPcH ligand. In permutations 1 and 2 of $[\mathbf{1}HH]^+$, the two α-obPcH ligands are chemically equivalent due to the presence of a C_2 symmetry axis, which goes through the Tb^{III} ion and is perpendicular to the vector that connects the two protons on the *meso*-N atoms.

3.3.2. Structural Changes Induced by Protonation. All the optimized structures showed that the α-omPc, α-omPcH, or α-omPcH$_2$ ligands are not in a completely staggered conformation, but rather slightly skewed away from the staggered conformation. These structures have, as the lowest vibrational mode, a libration toward the staggered conformation. This outcome of DFT geometry optimizations and frequency calculations was observed in our previous studies of β-obPc double-decker complexes.[7b] As described previously, the solution structure of these complexes, as observed on the NMR time scale, corresponds to a fully staggered conformation.

Generally, the DFT optimized geometries show that a protonation of only one phthalocyaninato ligand leaves the interligand distance almost unchanged. However, the metal-atom-to-ligand distance becomes inequivalent with a shorter distance to the doubly charged Pc^{2-} and longer to the PcH^- ligand (see the Supporting Information (Figure S24)). The $[Y(\alpha\text{-omPcH})_2]^+$ structures have a $d(Y^{III}-(\alpha\text{-omPcH}))$ of 1.39 Å, which is only slightly smaller than in the $[Y(\alpha\text{-omPc})_2]^-$ case (1.40 Å). In structures where only a single α-omPc ligand is protonated, the planarity of the nonprotonated α-omPc ligand is distorted to a concave shape, as a consequence of the reduced distance between this ligand and the metal center.

Previously, studies about the phthalocyaninato ligand rotation barriers in La^{III}–bis(phthalocyaninato) and in heteroleptic Ce^{IV}–(porphyrinato) (phthalocyaninato) double-decker complexes were conducted.[27] Studies of dynamics in lanthanoid complexes with porphyrinato ligands showed that the ligand rotation barriers can be large[24] and inversely proportional to the interplanar spacing between porphyrinato ligands.[25] We provide theoretical evidence that double protonation of the complex $[Tb(\alpha\text{-obPc})_2]^-$ ($[\mathbf{1}]^-$) results in a small contraction of the interligand distance (by ca. 0.02 Å). This contraction of the interligand distance is substantiated by an increase of the δ_{PC} of the protons on *meso*-N atoms in $[\mathbf{1}HH]^+[H\text{-DBU}]^-$, when compared to $[\mathbf{1}H]^0$. The DFT calculations also show that the two $[Y(\alpha\text{-omPcH})_2]^+$ structures have very similar energies, and a distinction between permutations 1 and 2 cannot be made based on the NMR data. With these results in mind, we propose that the dynamic process of $[\mathbf{1}HH]^+[H\text{-DBU}]^-$ which is observed at elevated temperatures, is due to a fast "hopping" of protons from one *meso*-N atom to another one, rather than being due to a lowered rotation barrier of the α-obPcH ligands induced by a change in the interligand distance. The mechanism of proton hopping could involve the energetically less favorable $[Y(\alpha\text{-omPcH}_2)(\alpha\text{-omPc})]^+$ structures (the structure described by permutation 3 contributes with 0.05% to the total population at 380.0 K, according to the Boltzmann distribution).

4. CONCLUSIONS

We report the preparation and characterization of the new complex $[Tb(\alpha\text{-obPc})_2H)]^0$ ($[\mathbf{1}H]^0$). The anionic ($[Tb(\alpha\text{-obPc})_2]^-$) and doubly protonated ($[Tb(\alpha\text{-obPcH})_2]^+$) complexes are easily obtainable by deprotonation with DBU or by a second protonation with acetic acid, respectively. Paramagnetic NMR, with the help of DFT calculations, has shown that the protonation of the anionic $[Tb(\alpha\text{-obPc})_2]^-$ double-decker

DOI: 10.1021/acs.inorgchem.5b02391
Inorg. Chem. 2015, 54, 11986–11992

complex happens on the *meso*-N atom, which is in agreement with other studies.[6] DFT calculations indicate that this protonation leads to an increased distance between the protonated ligand and the metal center, and to a decreased distance between the nonprotonated ligand and the metal center. A second proton can be attached to the *meso*-N atom of the other phthalocyaninato ligand. According to DFT calculations, and supported by increased experimental pseudo-contact shifts, the $[Tb(\alpha\text{-obPcH})_2]^+$ species has a slightly smaller interligand distance than $[Tb(\alpha\text{-obPc})_2]^-$. Detailed analysis of the SMM properties of $[Tb(\alpha\text{-obPc})_2]^-$, $[Tb(\alpha\text{-obPc})_2H]^0$, and $[Tb(\alpha\text{-obPcH})_2]^+$ is currently in progress.

■ ASSOCIATED CONTENT

Supporting Information

The Supporting Information is available free of charge on the ACS Publications website at DOI: 10.1021/acs.inorgchem.5b02391.

ESI-MS, IR, UV-vis-NIR spectra, crystal structure of ^1H, details about DFT calculations, ^1H NMR, ^{13}C NMR, 2D NMR correlation spectra (of $[\mathbf{1}H]^0$, $[\mathbf{1}]^-[HDBU]^+$, and $[\mathbf{1}HH]^+[CH_3COO]^-$) and additional information that is not listed in the main body of the paper. (PDF)

Crystallographic data regarding $C_{128}H_{160}N_{16}Tb$ (CIF)

■ AUTHOR INFORMATION

Corresponding Authors

*E-mail: kkatoh@m.tohoku.ac.jp (K. Katoh).
*E-mail: yamasita@agnus.chem.tohoku.ac.jp (M. Yamshita).
*E-mail: markus.enders@uni-heidelberg.de (M. Enders).

Notes

The authors declare no competing financial interest.

■ ACKNOWLEDGMENTS

We express our gratitude for the following research funds: a Ph.D. scholarship for M.D. from the Beilstein-Institut zur Förderung der Chemischen Wissenschaften, Grant-in-Aid for JSPS Fellows from Japan Society for the Promotion of Science (JSPS) (Y.H., T.M.), Tohoku University Division for International Advanced Research and Education (DIARE) (T.M.), a Grant-in-Aid for Scientific Research (S) (Grant No. 20225003, M.Y.), Grant-in-Aid for Young Scientists (B) (Grant No. 24750119, K.K.) and Scientific Research (C) (Grant No. 15K05467, K.K.) from the Ministry of Education, Culture, Sports, Science, and Technology, Japan (MEXT), and the German−Japanese University Consortium (HeKKSaGOn) for travel supports (all authors). We are grateful for the computational resources provided by the bwForCluster JUSTUS, funded by the Ministry of Science, Research and Arts and the Universities of the State of Baden-Württemberg, Germany, within the framework program bwHPC-C5.

■ REFERENCES

(1) Sessoli, R.; Gatteschi, D.; Caneschi, A.; Novak, M. A. *Nature* **1993**, *365*, 141−143.

(2) (a) Craig, G. A.; Murrie, M. *Chem. Soc. Rev.* **2015**, *44*, 2135−2147. (b) Meihaus, K. R.; Long, J. R. *Dalton Trans.* **2015**, *44*, 2517−28. (c) Tang, J.; Zhang, P., Lanthanide Single-Ion Molecular Magnets. In *Lanthanide Single Molecule Magnets*; Springer: Berlin, Heidelberg, Germany, 2015; pp 41−90. (d) Demir, S.; Jeon, I.-R.; Long, J. R.; Harris, T. D. *Coord. Chem. Rev.* **2015**, *289*−*290*, 149−176. (e) Feltham, H. L. C.; Brooker, S. *Coord. Chem. Rev.* **2014**, *276*, 1−33. (f) Liu, K.; Shi, W.; Cheng, P. *Coord. Chem. Rev.* **2015**, *289*−*290*, 74−122. (g) Dreiser, J. *J. Phys.: Condens. Matter* **2015**, *27*, 183203.

(3) (a) Ishikawa, N.; Sugita, M.; Ishikawa, T.; Koshihara, S.-y.; Kaizu, Y. *J. Am. Chem. Soc.* **2003**, *125*, 8694−8695. (b) Ishikawa, N.; Sugita, M.; Tanaka, N.; Ishikawa, T.; Koshihara, S.-y.; Kaizu, Y. *Inorg. Chem.* **2004**, *43*, 5498−5500.

(4) (a) Urdampilleta, M.; Klyatskaya, S.; Cleuziou, J. P.; Ruben, M.; Wernsdorfer, W. *Nat. Mater.* **2011**, *10*, 502−6. (b) Komeda, T.; Isshiki, H.; Liu, J.; Zhang, Y. F.; Lorente, N.; Katoh, K.; Breedlove, B. K.; Yamashita, M. *Nat. Commun.* **2011**, *2*, 217.

(5) Tanaka, D.; Inose, T.; Tanaka, H.; Lee, S.; Ishikawa, N.; Ogawa, T. *Chem. Commun.* **2012**, *48*, 7796−7798.

(6) Tanaka, D.; Sumitani, N.; Inose, T.; Tanaka, H.; Ishikawa, N.; Ogawa, T. *Chem. Lett.* **2015**, *44*, 668−670.

(7) (a) Damjanovic, M.; Katoh, K.; Yamashita, M.; Enders, M. *J. Am. Chem. Soc.* **2013**, *135*, 14349−14358. (b) Damjanović, M.; Morita, T.; Katoh, K.; Yamashita, M.; Enders, M. *Chem.—Eur. J.* **2015**, *21*, 14421−32.

(8) Gao, Y.; Li, R.; Dong, S.; Bian, Y.; Jiang, J. *Dalton Trans.* **2010**, *39*, 1321−1327.

(9) (a) Yongzhong, W.; He, T.; Kongchang, C.; Yunqi, L.; Daoben, Z. *Dyes Pigm.* **1998**, *37*, 317−325. (b) Galanin, N. E.; Shaposhnikov, G. P. *Russ. J. Gen. Chem.* **2012**, *82*, 1734−1739.

(10) Sheldrick, G. *Acta Crystallogr., Sect. A: Found. Crystallogr.* **2008**, *64*, 112−122.

(11) Findeisen, M.; Brand, T.; Berger, S. *Magn. Reson. Chem.* **2007**, *45*, 175−178.

(12) Fulmer, G. R.; Miller, A. J. M.; Sherden, N. H.; Gottlieb, H. E.; Nudelman, A.; Stoltz, B. M.; Bercaw, J. E.; Goldberg, K. I. *Organometallics* **2010**, *29*, 2176−2179.

(13) Holleman, A. F.; Wiberg, E.; Wiberg, N. *Lehrbuch der Anorganischen Chemie*, 101st Edition; Walter de Gruyter: Berlin, 1995.

(14) Frisch, M. J.; Trucks, G. W.; Schlegel, H. B.; Scuseria, G. E.; Robb, M. A.; Cheeseman, J. R.; Scalmani, G.; Barone, V.; Mennucci, B.; Petersson, G. A.; Nakatsuji, H.; Caricato, M.; Li, X.; Hratchian, H. P.; Izmaylov, A. F.; Bloino, J.; Zheng, G.; Sonnenberg, J. L.; Hada, M.; Ehara, M.; Toyota, K.; Fukuda, R.; Hasegawa, J.; Ishida, M.; Nakajima, T.; Honda, Y.; Kitao, O.; Nakai, H.; Vreven, T.; Montgomery Jr., J. A.; Peralta, J. E.; Ogliaro, F.; Bearpark, M. J.; Heyd, J.; Brothers, E. N.; Kudin, K. N.; Staroverov, V. N.; Kobayashi, R.; Normand, J.; Raghavachari, K.; Rendell, A. P.; Burant, J. C.; Iyengar, S. S.; Tomasi, J.; Cossi, M.; Rega, N.; Millam, N. J.; Klene, M.; Knox, J. E.; Cross, J. B.; Bakken, V.; Adamo, C.; Jaramillo, J.; Gomperts, R.; Stratmann, R. E.; Yazyev, O.; Austin, A. J.; Cammi, R.; Pomelli, C.; Ochterski, J. W.; Martin, R. L.; Morokuma, K.; Zakrzewski, V. G.; Voth, G. A.; Salvador, P.; Dannenberg, J. J.; Dapprich, S.; Daniels, A. D.; Farkas, Ö.; Foresman, J. B.; Ortiz, J. V.; Cioslowski, J.; Fox, D. J. *Gaussian 09, revision D.01*; Gaussian, Inc.: Wallingford, CT, USA, 2009.

(15) (a) Becke, A. D. *J. Chem. Phys.* **1993**, *98*, 5648−5652. (b) Lee, C.; Yang, W.; Parr, R. G. *Phys. Rev. B: Condens. Matter Mater. Phys.* **1988**, *37*, 785−789.

(16) (a) Weigend, F.; Ahlrichs, R. *Phys. Chem. Chem. Phys.* **2005**, *7*, 3297−3305. (b) Weigend, F. *Phys. Chem. Chem. Phys.* **2006**, *8*, 1057−1065.

(17) (a) Bergner, A.; Dolg, M.; Küchle, W.; Stoll, H.; Preuß, H. *Mol. Phys.* **1993**, *80*, 1431−1441. (b) Kaupp, M.; Schleyer, P. v. R.; Stoll, H.; Preuss, H. *J. Chem. Phys.* **1991**, *94*, 1360−1366. (c) Dolg, M.; Stoll, H.; Preuss, H.; Pitzer, R. M. *J. Phys. Chem.* **1993**, *97*, 5852−5859.

(18) (a) Grimme, S.; Ehrlich, S.; Goerigk, L. *J. Comput. Chem.* **2011**, *32*, 1456−1465. (b) Grimme, S., Dispersion Interaction and Chemical Bonding. In *The Chemical Bond*; Wiley−VCH Verlag GmbH & Co. KGaA: Weinheim, Germany, 2014; pp 477−500.

(19) Bacskay, G. B. *Chem. Phys.* **1981**, *61*, 385−404.

(20) Kitagawa, Y.; Kawakami, T.; Yamanaka, S.; Okumura, M. *Mol. Phys.* **2014**, *112*, 995−1001.

DOI: 10.1021/acs.inorgchem.5b02391
Inorg. Chem. 2015, 54, 11986−11992

(21) Bertini, I.; Luchinat, C.; Parigi, G. *Solution NMR of Paramagnetic Molecules—Applications to Metallobiomolecules and Models*; Elsevier: Amsterdam, 2001.
(22) La Mar, G. N. *NMR of Paramagnetic Molecules—Principles and Applications*; Academic Press: New York and London, 1973.
(23) (a) Kaupp, M.; Köhler, F. H. *Coord. Chem. Rev.* **2009**, *253*, 2376−2386. (b) Köhler, F. H. Paramagnetic Complexes in Solution: The NMR Approach. In *eMagRes*; John Wiley & Sons, Ltd.: New York, 2007. (c) Piguet, C.; Geraldes, C. F. G. C. Paramagnetic NMR Lanthanide Induced Shifts for Extracting Solution Structures. In *Handbook on the Physics and Chemistry of Rare Earths*; Gschneidner, K. A., Jr., Bunzli, J.-C. G., Pecharsky, V. K., Eds.; Elsevier: Amsterdam, 2003; Vol. *33*, pp 353−463. (d) Soncini, A.; Van den Heuvel, W. *J. Chem. Phys.* **2013**, *138*, 021103. (e) Gendron, F.; Sharkas, K.; Autschbach, J. *J. Phys. Chem. Lett.* **2015**, *6*, 2183−2188. (f) Gendron, F.; Pritchard, B.; Bolvin, H.; Autschbach, J. *Dalton Trans.* **2015**, *44*, 19886.
(24) Tashiro, K.; Konishi, K.; Aida, T. *J. Am. Chem. Soc.* **2000**, *122*, 7921−7926.
(25) Babailov, S. P. *Prog. Nucl. Magn. Reson. Spectrosc.* **2008**, *52*, 1−21.
(26) Gendron, F.; Páez-Hernández, D.; Notter, F.-P.; Pritchard, B.; Bolvin, H.; Autschbach, J. *Chem.—Eur. J.* **2014**, *20*, 7994−8011.
(27) (a) Qi, D.; Zhang, L.; Wan, L.; Zhang, Y.; Bian, Y.; Jiang, J. *Phys. Chem. Chem. Phys.* **2011**, *13*, 13277−13286. (b) Otsuki, J.; Taka, M.; Kobayashi, D. *Chem. Lett.* **2011**, *40*, 717−719.

DOI: 10.1021/acs.inorgchem.5b02391
Inorg. Chem. 2015, 54, 11986−11992